Article

Travelling Surface Plasmons with Interference Envelope and A Vision for Time Crystals

Amir Djalalian-Assl [1,*]

[1] ORCID:0000-0002-7132-1085
* Correspondence: amir.djalalian@gmail.com

Abstract: The influence of the film thickness and the substrate's refractive index on the surface mode at the superstrate is an important study step that may help clearing some of the misunderstandings surrounding their propagation mechanism. A single sub-wavelength slit perforating a thin metallic film is among the simplest nanostructure capable of launching Surface Plasmon Polaritons on its surrounding surface when excited by an incident field. Here, the impact of the substrate and the film thickness on surface waves is investigated. When the thickness of the film is comparable to its skin depth, SPP waves from the substrate penetrate the film and emerge from the superstrate, creating a superposition of two SPP waves, that leads to a beat interference envelope with well-defined loci which are the function of both the drive frequency and the dielectric constant of the substrate/superstrate. As the film thickness is reduced to the SPP's penetration depth, surface waves from optically denser dielectric/metal interface would dominate, leading to volume plasmons that propagate inside the film at optical frequencies. Interference of periodic volume charge density with the incident field over the film creates charge bundles that are periodic in space and time.

Keywords: surface plasmons; time crystal; thin film

1. Introduction

In a most relevant report (to a certain extent) Wang *et. al.*[1] modelled a free standing optically thin silver film in vacuum, where authors try to explain their findings in terms of long range SPPs, SPP Wave Packets and Quasi Cylindrical Waves (QCW) … etc. Prior to that, Verhagen *et. al.* showed that guided waves in a metal-dielectric-metal waveguide can penetrate the thin metallic cladding hence shortening the wavelength of the SPPs at the silver/air interface [2].

When the refractive index of the substrate differs from that of the superstrate, however, the superposition of the two waves from both sides of the film leads to travelling SPP waves modulated by a well define non-travelling interference envelope at metal/dielectric interfaces. For a sufficiently thin metallic layer, SPPs formed at the metal/superstrate also interfere with those formed at the metal/substrate within the metal leading to a non-travelling periodic electric polarization inside the film. Note that this report is not concerned with the SPP eigenmodes [3-5], but rather it is an investigation on surface wave interference under the forced vibration. The numerical results reported here are exactly those included in chapter 10 of my thesis [6]. However, during the internal review, pre- and post-examination period of my thesis, it was requested that I remove the notions of Lorentz force and periodic transparency. This version of the report has those notions restored and used for explaining the mechanism behind the plasmonic time-crystal and more.

Let us start with the fundamental equations governing the surface plasmons polaritons (SPP) stated here for convenience [7]:

$$k_{SPP} = \sqrt{\frac{\varepsilon_m \varepsilon_d}{\varepsilon_m + \varepsilon_d}} k \equiv k'_{SPP} + \mathrm{i}\, k''_{SPP} \qquad (1)$$

$$k_m \approx \sqrt{\frac{\varepsilon_m^2}{\varepsilon_m + \varepsilon_d}} k \equiv k'_m + \mathrm{i} k''_m \qquad (2)$$

 doi:10.20944/preprints201801.0173.v4

There is also a very useful presentation by Rosa [8] that would help the reader to gain background knowledge on SPPs. Not having access to the university resource, I could not cite the references in that presentation. So, I hope citing Rosa's work would suffice for now.

Now, consider a metallic thin film with its surface set parallel to the *x*-*y* plane. Equation (1) describes the complex wave vector for the SPP waves propagating at the metal/dielectric interface along the *x*-*y* plane, whereas the wave vector for the SPP waves penetrating the metallic film in the *z*-direction is given by equation (2). In both equations the real part of the wave vector represents propagation constant, whereas the imaginary part defines the decay lengths, $1/k''_{SPP}$ and $1/k''_m$, over which the SPP's amplitude decreases by 1/*e*. Note that in equation (2), the permittivity, ε_d, corresponds to the dielectric material from which the field penetrates the film.

The short introduction above was aimed to highlight some of the key features of surface plasmon polaritons relevant to this report. What will follow is a theoretical study on SPPs launched by a single subwavelength aperture perforated in a silver thin film. Section 2.1 covers the influence of the film thickness and the refractive index of the supporting substrate on the SPPs and in section 2.2 a plasmonic time crystal is proposed.

2. Results and Discussions

2.1 The Origin of Modulating Envelope in SPPs over Flat Metallic Films

A 2D Finite Element Method (FEM) model of a 100 nm thick silver film perforated with a 50 nm wide slit was simulated. Modelling time harmonics with FEM is particularly useful in examining the steady-state response of the system under the continues excitation with an incident wave with a single wavelength. The refractive index of the glass substrate supporting the film was initially set to $n_1 = 1.52$ and the refractive index data for silver was taken from Palik [9]. The film was along the *x* plane and was illuminated with a normally incident TM wave propagating in the +*z*-direction from glass substrate. For convenience the air/silver interface is denoted by $z = z_0$. Figure 1(a) depicts the distribution of the real part of surface charge densities, $\sigma(x,t) = |\sigma(x)|e^{i(k_{SPP}x-\omega_0 t)}$, at an arbitrary time t_0, calculated at both the air/silver and glass/silver interfaces from the normal to the surface, i.e. the *z*-component of the electric field. The amplitude, i.e. the envelope, of the surface charge density at the air/silver interface was calculated using $|\sigma(x)| = \sqrt{\sigma(x,t)\sigma(x,t)^*}$ and is depicted in Figure 1(b). The corresponding Fast Fourier Transforms (FFT), $f[\sigma(x,t_0)]$ and $f[|\sigma(x)|]$ were also calculated, see Figure 1(c)-(d).

Preprints (www.preprints.org) | NOT PEER-REVIEWED | Posted: 29 April 2018 doi:10.20944/preprints201801.0173.v4

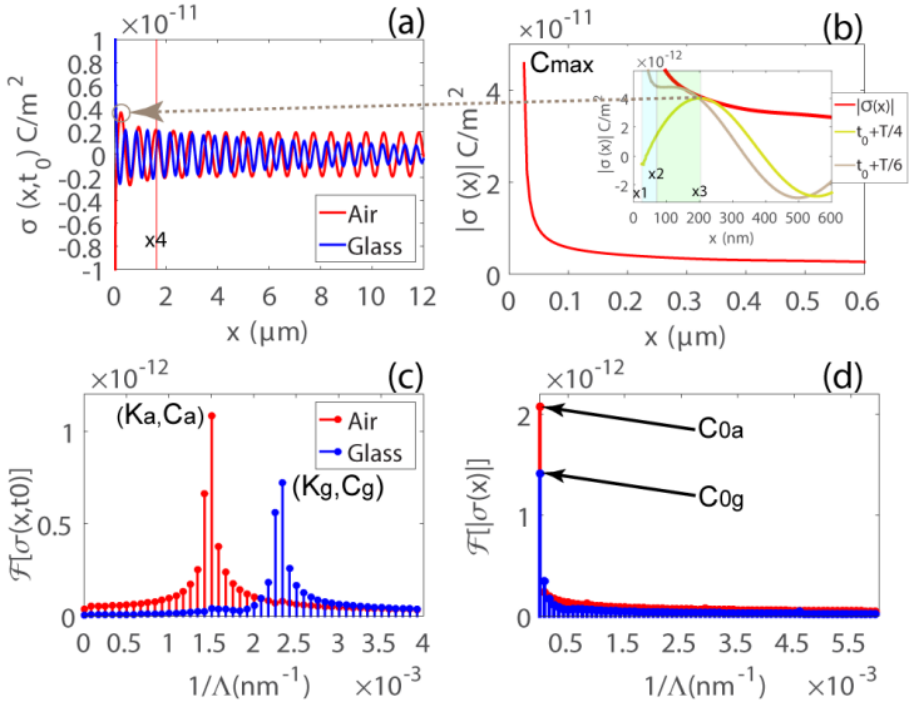

Figure 1: (a) Surface charge density, $\sigma(x, t_0)$, at an arbitrary time t_0, calculated at the air/silver and glass/silver interfaces. (b) The envelope, $|\sigma(x)|$, at the air/silver interface. The corresponding FFT of (c) the wave $f\left[\sigma\left(x,t_0\right)\right]$ and (d) the envelope $f\left[\left|\sigma\left(x\right)\right|\right]$ [6].

In Figure 1(b), the maximum accumulated charge density at the edge of the cavity, $x_1 = 25$ nm, is labelled C_{max}. The decay length of the surface charge density, where the value of the C_{max} drop by $1/e$, was found to be ~10 nm from the edge (or 35 nm from the center). At $\lambda_0 = 700$ nm, the decay length of an SPP along the silver/air interface is ~67 μm [7]. Activities near the slit, therefore, may not be considered as SPPs as they are highly localized. The inset of Figure 1(b), depict the $|\sigma(x)|$ and $\sigma(x,t)$ at $t = t_0 + T/6$ and $t_0 + T/4$. Here, T is the period and t_0 was set to a time when the surface charge density was at its maximum, C_{max}, at x_1. The separation between the localized surface charges and the appearance of the harmonic wave occurs at $t = t_0 + T/6$ and $x_2 \approx 75$ nm, i.e. 50 nm away from the edge. In fact, the 10 nm decay length, closer to the $1/k_m'' \approx 25$ nm obtained from equation (2), indicates that the surface charges in the vicinity of the slit are due to the cavity modes, penetrating the metal and subsequently decaying rapidly. This agrees to previous works [10,11]. Furthermore, at $t = t_0 + T/4$ the surface charge density at x_1 drops to 0 and the peak at $x_3 = 200$ nm resembles that of a harmonic wave. The phase difference of 90° between the oscillations at x_1 and x_3, resembles that of a forced vibration where the force leads the displacement by 90° under resonance conditions [12]. However, the amplitude of the first peak at x_3 is $1.9\times C_{0a}$, where C_{0a} is the DC component of $|\sigma(x)|$, hence the average amplitude of the travelling SPP waves, see Figure 1(a) and (d). Note FFT of the envelope, $f\left[\left|\sigma\left(x\right)\right|\right]$, in Figure 1(d), identifies the DC components (or the amplitudes of the SPP waves), C_{0a} and C_{0g} at both interfaces.

By examining Figure 1(a) it was determined that the amplitude of the wave drops to C_{0a} at $x_4 \approx w/2 + 2\times\lambda_{SPP}$, i.e. 2 wavelengths away from the edge of the slit. Although the surface charge density resembles that of a harmonic oscillation in the $x_3 \le x \le x_4$ range, its rapid decay and non-conformance to the $1/k_{SPP}''$, suggests a kind of transient state. To evaluate the λ_{SPP}, FFT transform $f\left[\sigma\left(x,t_0\right)\right]$ was calculated for both the silver/air and the silver/glass interfaces, Figure 1(c). The weighted average, $K_{SPP} = \sum_{i=1}^{5}\left(K_{SPPi}C_{SPPi}\right)/C_{SPPi}$, that included the center mode and the four immediate neighboring modes, i.e. two on each side of the maxima, provides a good estimate of SPP wavenumbers. The SPP

Preprints (www.preprints.org) | NOT PEER-REVIEWED | Posted: 29 April 2018 doi:10.20944/preprints201801.0173.v4

wavelengths were then calculated using $\lambda_{SPP} = 1/K_{SPP}$, where $K_{SPP} = \mathrm{Re}(k_{SPP})/2\pi$ is the wavenumber obtained from FFT.

For the sake of brevity in notations, let the subscripts "*a*" and "*g*" be denoting the association of physical quantities carried by the SPP waves at the superstrate (air) and substrate (glass and later diamond) respectively. So, in summary, $\lambda_a = 1/K_a = 667$ nm and $\lambda_g = 1/K_g = 427$ nm are in agreement with $\lambda_a = 682$ nm and $\lambda_g = 433$ nm obtained analytically using equation (1). Examining the $|\sigma(x)|$, an additional spatial second harmonic were observed in the envelope at both interfaces. The second harmonics in the envelope seems to be the result of superposition of two time-harmonic waves:

$$\sigma(x,t) = E_z e^{i(k_a x - \omega_0 t)} + E_{z?} e^{i(-k_a x - \omega_0 t + m\pi)} \qquad (3)$$

where m must be an even integer and $E_z >> E_{z?}$. However, the origin of the second term in equation (3) , $E_{z?}$, is unknown. The boundary conditions were set to eliminate all reflections, therefore, simulation artefacts cannot account for such periodic perturbations, even more so that such second harmonics do not manifest themselves over the surface of a Perfect Electric Conductor (PEC) that does not support SPPs!

A possible scenario that may lead to oscillations at double the fundamental frequency in $|\sigma(x)|$, is the normal-to-the-surface component of SPPs being modulated by the parallel-to-the-surface component at the interface via a relationship that involved multiplication. SPPs are longitudinal waves manifested as surface charge bundles, where charges in each bundle are held together by SPP's E_z along the x-axis. Repelling/attracting Coulomb forces from each bundle to its neighboring charge bundles of equal/opposite signs, is analogous to a chain of masses attached to one another by springs. Given that the oscillation along the chain is being driven by $F \propto \sigma(x,t) E_x(z_0,t)$ from the aperture, it is plausible to attribute the origin of the backward propagating term in equation (3) to $F_x \propto e^{-i2(k_a x - \omega_0 t)}$, where the push/pull by F_x generates the backward propagating waves. Basically, the force modulates the amplitude of the surface charge density wave over $T/2$, during which the SPP has travelled a total distance of $\lambda_g/2$. Having noted that, the exact form of a partial differential equation governing the forced vibration that leads to equation (3) as a solution is yet to be determined.

Regardless, it was envisaged that by reducing the film thickness, it would be possible for surface charge densities from the glass/silver interface manifest themselves at the air/silver interface, leading to a superposition of the two waves:

$$\sigma(x) = \left[2e^{i\left(\frac{(k_a + k_g)x}{2}\right)} \cos\left(\frac{(k_a - k_g)x}{2}\right) \right] \qquad (4)$$

see Appendix A. This would modulate the charge densities along the *x*-direction, resulting in a series of minima/maxima with fixed loci that are $1/K_{beat}$ apart, where $K_{beat} \equiv |K_a - K_g|$. Hence by controlling the film thickness and the refractive index of the substrate, one could control the modulation strength and frequency of the envelope. Keeping the superstrate and the substrate intact as before, two additional simulations, with $h = \{50, 25\}$ nm, were carried out in order to investigate the influence of the film thickness. Figure 2 depict the numerically calculated $f\left[\sigma(x,t_0)\right]$ and $f\left[\left|\sigma(x)\right|\right]$. Figure 2(a), (c) and (e) depicts $f\left[\sigma(x,t_0)\right]$ with $h = \{50, 25\}$ nm when the film is supported on a glass substrate and with $h = 25$ nm on a diamond substrate respectively. In all cases, K_a was found to be at the same position as it was for $h = 100$ nm. For $h = \{50, 25\}$ nm on a glass substrate, K_g was also found to be at the exact location as it was for the 100 nm thick silver film. In the case of the diamond substrate, $\lambda_g = 1/K_g = 230$ nm, was found to be close to the $\lambda_g = 246$ nm calculated using equation (1) . In all cases, the appearance of an additional peak at the air/silver interface, positioned at K_g having an amplitude $C_{\delta g} = C_g e^{-\frac{z}{\delta}}$, corresponded to the SPP waves that travel along the substrate/silver interface penetrating the film and emerging at the air/silver interface. Presence of SPPs with wavelength λ_g at air/silver interface is significant as it impacts the design criteria for plasmonic meta-

Preprints (www.preprints.org) | NOT PEER-REVIEWED | Posted: 29 April 2018 doi:10.20944/preprints201801.0173.v4

surfaces. FFT of the corresponding envelopes, $f\left[\left|\sigma(x)\right|\right]$, in Figure 2(b), (d) and (f), show the anticipated modulating envelope with $K_{beat} \equiv |K_a - K_g|$.

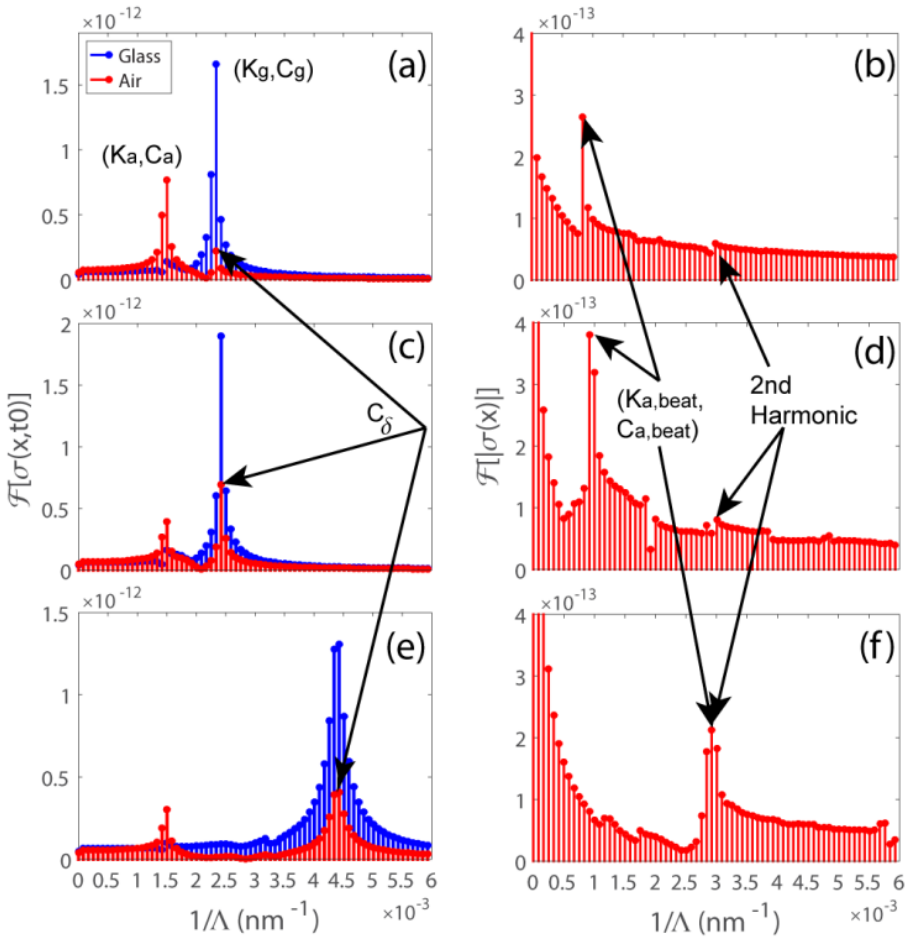

Figure 2: $f\left[\sigma\left(x,t_0\right)\right]$ and $f\left[\left|\sigma(x)\right|\right]$ calculated for (a)-(b) h = 50 nm on glass substrate, (c)-(d) h = 25 nm on glass substrate and (e)-(f) h = 25 nm on diamond substrate. Note that subscript 'g' is used to label the substrate in general [6].

Note that in order to shift the K_{beat} to overlap with the second harmonics observed in the envelope, the required value for the substrate's refractive index was found to be (see Appendix A) n_1 = 2.41 at λ_0 = 700 nm that corresponds to diamond [13]. With the recent advances in nano-diamond technology, use of diamond substrate is both feasible and practical [14]. Therefore, an additional simulation was carried out with a 25 nm thick silver film supported on a diamond substrate.

Figure 3 depicts the modulating envelopes, $|\sigma(x)|$, calculated over the air/silver interface for h = {100, 50, 25} nm when the film is supported on a glass substrate and for h = 25 nm with a diamond substrate. The aperture was normally illuminated with a Gaussian beam, 15×λ_0 in waist, from the substrate. The surface of a perfect electric conductor (PEC) that neither supports SPPs nor allows the penetration of the fields, produced only a smooth line, see Figure 3-(line in black). Values for the PEC line were calculated using $\varepsilon_0 E_z$ to retain the C/m² unit. The inset in Figure 3 shows the travelling SPPs, $\sigma(x, t)$, that are modulated by the envelope $|\sigma(x)|$, calculated over the air/silver interface for the case h = 50 nm when excited with a plane wave from the glass substrate. The presence of the second harmonic and the beat interference in the envelope are marked.

Preprints (www.preprints.org) | NOT PEER-REVIEWED | Posted: 29 April 2018 doi:10.20944/preprints201801.0173.v4

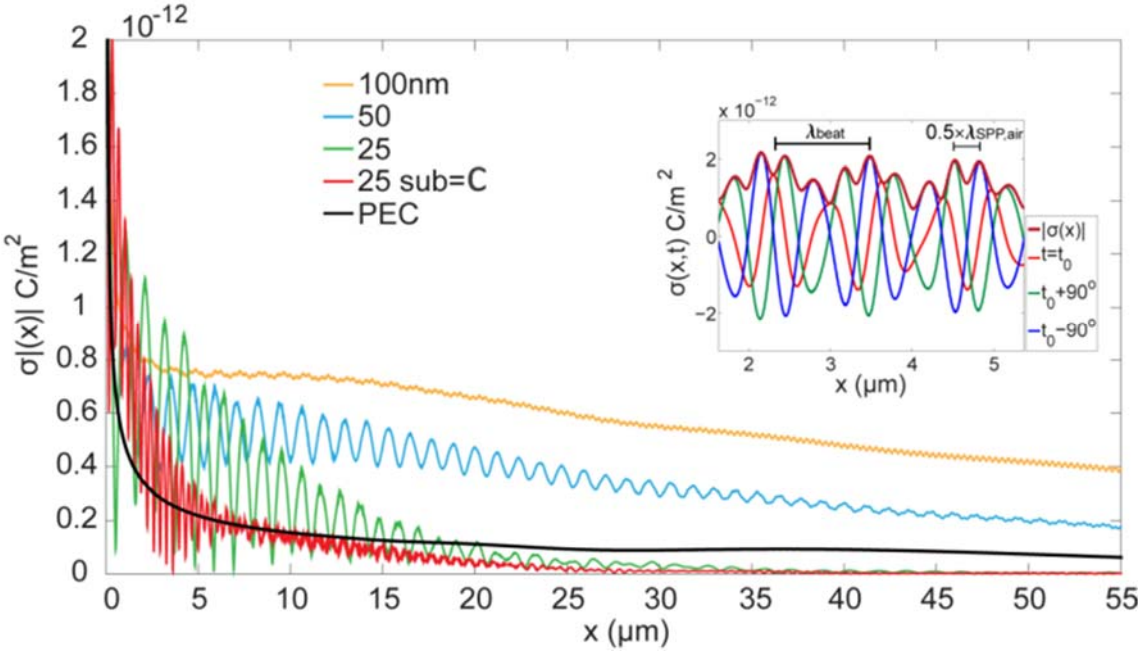

Figure 3: Surface charge densities, $|\sigma(x)|$, over the air/silver surface for h = {100, 50, 25} on glass substrate, h = 25 nm on diamond substrate and for PEC [6].

A noticeable feature in Figure 3 is the relation between the SPP's decay length, $1/k''_{SPP}$, along the air/silver interface and the strength (or the amplitude) of the interference envelope. Travelling SPP waves along the air/silver interface may be described as the superposition of two waves according to equation (A4) in Appendix A, where each component decay according to their respective decay length $1/k''_a$ and $1/k''_g$. Analytical values for decay lengths were found to be {67, 17, 3.2) μm for the air/silver, glass/silver and diamond/silver interfaces respectively. This explains the decay length of the envelope clearly. For example, in the case of the 25 nm silver film supported on a diamond substrate, the amplitude of the $C_{\delta g}e^{i(k_g x-\omega_0 t)}$ component drops to 1/e of its maximum at x = 3.2 μm, beyond which the only component that continues to propagate is $C_{0a}e^{i(k_a x-\omega_0 t)}$ due to its longer decay length of ~67 μm. And since the modulating envelope with K_{beat} requires the presence of both components at the air/silver interface, the decay length of the envelope is dictated by the component having the shortest of the two decay lengths, which in this example is 3.2 μm associated with the $C_{\delta g}e^{i(k_g x-\omega_0 t)}$. Experimental measurements of such effects, however, may not be possible. Although measurements carried out by Verhagen *et. al.* [2] *may* be valid, Wang *et. al.*[1] correctly pointed out that positioning any probe such as an AFM tip, in the vicinity of the slit stablishes standing wave oscillations between the tip and the slit, leading to a series of minima/maxima that convolve with those of the interference envelope. FEM simulations has confirmed this.

The concept of plasmonic microzones [15,16] are not something new. What sets apart what I have reported here is the formation of the periodic screening/transparency (i.e. the zone plate) by the SPPs alone, and not during the fabrication. For the diamond substrate, diffraction patterns through a 25 nm silver film with single hole when excited with a normally incident beam (Gaussian in x) having a waist of $2\times\lambda_0$, is shown in Figure 4(a). When the maximum intensity of the Gaussian beam falls away from the centre of the slit (an arbitrary displacement of 680 nm in this case) the intensity of the transmitted beam exhibits a curvature and a tilt towards the displacement, with the transmitted beam being split in two, Figure 4(b). Such light-matter interaction is not observed in the transmitted beam through a 25 nm silver film on a diamond substrate with no aperture, see Figure 4(c).

Preprints (www.preprints.org) | NOT PEER-REVIEWED | Posted: 29 April 2018 doi:10.20944/preprints201801.0173.v4

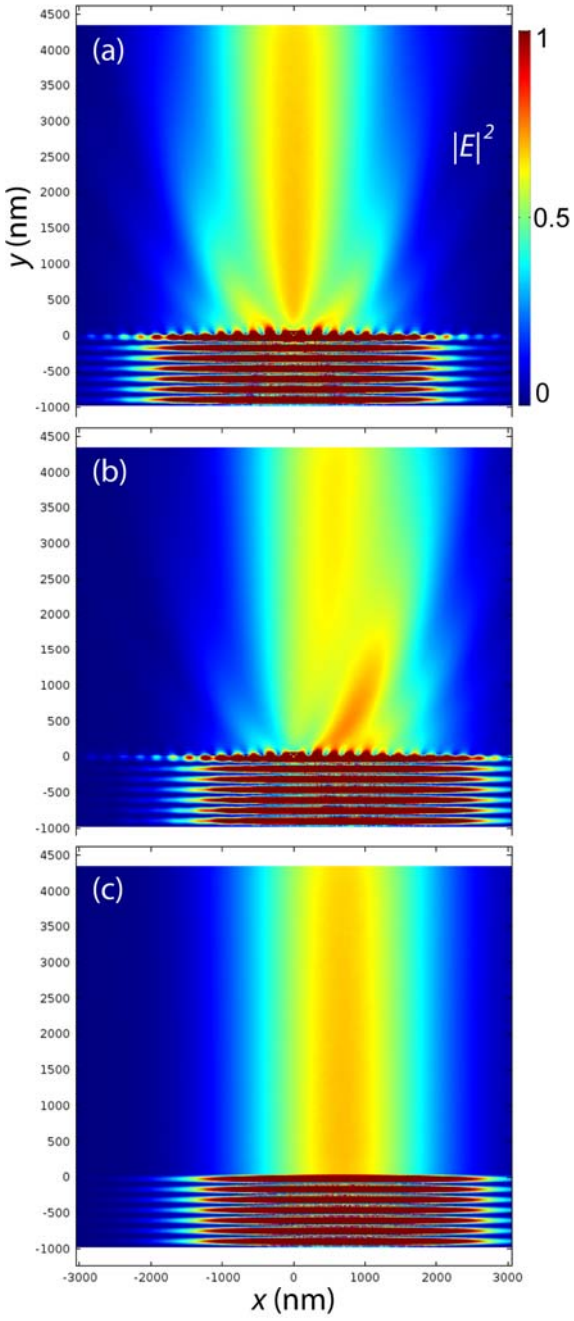

Figure 4: $|E|^2 \times 10(\mathrm{V/m})^2$ Diffraction patterns of a transmitted Gaussian beam through (a) 25 nm silver film perforated with a slit, supported on a diamond substrate. (b) same as (a) with the maximum intensity of the Gaussian beam displaced to x = 680 nm away from the centre of the slit. (c) In the absence of the slit [6].

2.2 Roadmap to Further Study and a Vision for Plasmonic Time Crystal

With diamond (or glass) substrate, when the film thinness is that of the skin depth, SPPs are no longer confined to the surface of the metal but rather penetrate the film from the substrate and superstrate and interfere with one another inside the film. However, (as it is the case here), due to the aperture dimensions and partially due to the $\varepsilon_m E_{zm} = \varepsilon_d E_{zd}$ [8], normal to the surface component of the electric field at the diamond/silver boundary is much stronger than those at the air/silver at $\lambda_0 = 700$ nm, hence $E_{zg} >> E_{za}$. Therefore, fields from the substrate dominate the film. Furthermore, the x-component of the SPP was found to be stronger than its z-components at $\lambda_0 = 700$ nm, i.e.

Preprints (www.preprints.org) | NOT PEER-REVIEWED | Posted: 29 April 2018 doi:10.20944/preprints201801.0173.v4

$E_{xg} \approx 2E_{zg}$ calculated using $E_{xg} = -i\sqrt{\frac{-\varepsilon_m}{\varepsilon_d}}E_{zg}$ [8], and in agreement with the numerical results. Furthermore a trail of *z*-component of the electric field {…0 – 0 + 0 – 0 …} carries a trail of *x*-component {… – 0 + 0 – 0 + …} with "+", "0" and "-" denoting $+E_{x,z}$, 0 and $-E_{x,z}$ respectively. Note the 90° phase difference between the *x* and the *z*-components. Naturally, the induced periodic polarization, travels inside the film as the SPPs propagate over the surface. The *x*-component of the polarization, $P_{xg} = \varepsilon_0 \chi_e E_{xg} e^{i(k_g x - \omega_0 t)}$, is of interest in the context of plasmonic time crystals as it signifies periodic accumulation of conduction electrons along the *x*-axis, hence periodic screening/transparency within the film that resembles that of a Fresnel zone plate.

With a flat metallic film that extends to infinity in the *x*-direction, it is not possible to apply the Gauss's law to calculate the charges due to SPP fields. Therefore, I have provided an alternative approach to calculate the induced periodic charge density due to propagating E_{zg}:

$$\Delta\rho_x(k_g, \omega_0) = -\frac{\omega_0}{c}\varepsilon_0 \varepsilon_m^{"}\left[\frac{\varepsilon_d + \varepsilon_m}{\sqrt{\varepsilon_m + \varepsilon_d}}\right]E_{zg}e^{i(k_g x - \omega_0 t)} \qquad (5)$$

see Appendix B. And in terms of number of electrons being displaced:

$$\Delta N(k_g, \omega_0) = \frac{\Delta\rho_x}{e^-} = -\frac{\omega_0}{ce^-}\varepsilon_0 \varepsilon_m^{"}\left[\frac{\varepsilon_m + \varepsilon_d}{\sqrt{\varepsilon_m + \varepsilon_d}}\right]E_{zg}e^{i(k_g x - \omega_0 t)} \qquad (6)$$

Equation (6) reveals the total number of charges being displaced per SPP field. Given that the fermi energy level for metals is given by $\mathcal{E}_F = \frac{h^2}{8m}\left(\frac{3N}{\pi}\right)^{2/3}$ [17], one must set $N = N_0 + \Delta N$, where N_0 is the number of electrons per unit volume when unperturbed.

$$\mathcal{E}_F(k_g, \omega_0) = \frac{3^{2/3}h^2}{8m\pi^{2/3}}\left(N_0 + \Delta N\right)^{2/3} \qquad (7)$$

Consequently, $\Delta\rho_x$, ΔN and $\mathcal{E}_F$ become a function (k_g, ω_0) due to $E_{zg}e^{i(k_g x - \omega_0 t)}$, which may lead to many interesting effects, such as periodic refractive index, fermi levels, local work functions, density of states, eigen energies inside film, which will be a topic of another report. Nevertheless, in the absence of any incident field over the film, for example when the SPPs are launched by a dipole near the surface [18], the propagation of surface waves, and all physical quantities they carry, is unperturbed. However, in the presence of an incident field normal to the surface, the superposition of the fields inside the film is given by $E = E_{xi}e^{i(k_i z - \omega_0 t)} + E_{xg}e^{i(k_g x - \omega_0 t)}$ which create disturbance on the periodic charges densities. It is intuitive that loci polarized by $+E_{xg}$ be transparent to $+E_{xi}$, and vice versa. Now, consider an arbitrary time $t = t_0$, when the maximum of the incident electric field falls over the film. This is depicted by the following notation:

$$\frac{E_{xg}(x, t_0): +, 0, -, 0, +}{E_{xi}(t_0): +, +, +, +, +} \Rightarrow +, +, 0, +, + \qquad (8)$$

This scenario is shown in Figure 5 with the periodic arrangement of "0"s when the maximum of the field falls over the film. Also note the strong periodic field under the film, inside the glass and diamond substrates! At $t = t_0 + T/2$, hence 180° phase, both E_{xg} and E_i change sings. This will lead to:

$$\frac{E_{xg}(x, t_0 + T/2): -, 0, +, 0, -}{E_{xi}(t_0 + T/2): -, -, -, -, -} \Rightarrow -, -, 0, -, - \qquad (9)$$

Preprints (www.preprints.org) | NOT PEER-REVIEWED | Posted: 29 April 2018 doi:10.20944/preprints201801.0173.v4

with "0" remained intact in space as it was in the case of equation (8). This scenario is also confirmed by numerical results.

It is intuitive to think of the periodic "0"s as loci where conduction electrons are trapped. If this hypothesis is validated by experiment, it would open doors to study new phenomena. Each "0" may be viewed as a super-atom with oversaturated electronic orbitals, elevated fermi level, lowered work function and many more effects when considered in periodic settings which I have highlighted in the conclusion.

Back to causality, at the first glance it seems it is a simple matter of superposition of two orthogonally propagating EM waves with the *x*-component of the two fields summed up inside the film. However, a close look at the numerical results revealed that when E_{xi} drops to 0, (e.g. at $t = t_0+T/4$), polarization inside the film experiences the effect of $E_{xi}(t_0)$. This 90° phase difference between applied filed and the reaction is attributed to the charge bundles experiencing the Lorentz force $F_{xg} = J_{zg}(B_{yg} + B_{yi})$. Furthermore, since B_{yi} is 0 at $t = t_0+T/4$, the restoration of periodic potential is resumed at $t = t_0+T/4$ but completed at $t = t_0+T/2$ when $-E_{xi}$ falls over the film. The whole creation/anhelation of $P_x = \varepsilon_0 \chi_e E_x$ is a sinusoidal process in time. Numerical results also revealed that E_{zg} not being affected by the *incident* field. Therefore, the restoration process is attributed to the E_{zg}. Since this creation/anhelation is periodic both in time and space with periodicities $T/2$ and λ_g, hence oscillating at frequency other than that of the drive, (although not an expert in the topic), I believe it qualifies as a time crystal [19,20]. As for the breaking time symmetry, I need access to certain resources only academics enjoy, but as an alumnus, this is not possible at this stage. However, I must remind the readers that the *x*-component of the SPP's electric field (as I understand) must always lag its *z*-components by 90° at *resonance*, a condition satisfied for SPPs launched by an aperture at any frequency.

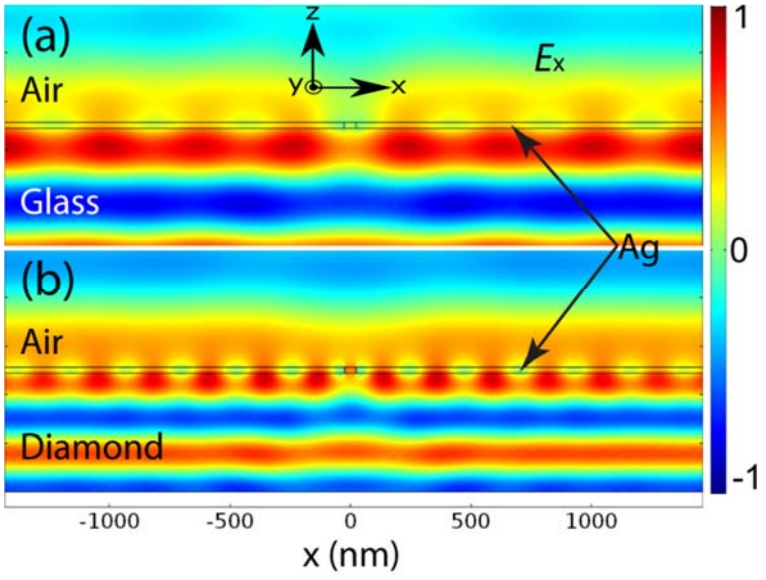

Figure 5: Snapshot of electric field E_x passing through a periodic charge screen (with periodicity $1/K_g$) formed inside the 25 nm thick silver film for (a) glass and (b) diamond substrates. Note that E_x was calculated at an arbitrary time with the maximum of its amplitude falling over the silver film [6].

The term *crystal* also implies that one should be able to define both the Hamiltonian to determine the eigen-energies and the Schrödinger equation to explain the De Broglie's matter waves [21,22] for that system. The potentials *V*, experienced by electrons in a time crystal and consequently, wave functions ψ and eigen-energies ξ, must naturally be time-dependent:

$$\xi_j(t)\psi_j\left(\mathbf{R}_j,t\right) = \hat{H}(t)\psi_j\left(\mathbf{R}_j,t\right) \qquad (10)$$

Preprints (www.preprints.org) | NOT PEER-REVIEWED | Posted: 29 April 2018 doi:10.20944/preprints201801.0173.v4

$$i\hbar\frac{\partial\psi_j(\mathbf{R}_j,t)}{\partial t}=\hat{H}(t)\psi_j(\mathbf{R}_j,t) \qquad (11)$$

Considering the original Hamiltonian, $\hat{H}$, for the many-electrons [23]:

$$\hat{H}=\sum_j\left[-\frac{\hbar^2}{2m}\nabla_j^2+V(\mathbf{R}_j)\right]+\frac{1}{2}\sum_{\substack{j,k\\ j\neq k}}\frac{e^2}{4\pi\varepsilon|\mathbf{R}_j-\mathbf{R}_k|} \qquad (12)$$

Time variations of kinetic energy term in equation (12) is taken care of by the time-dependent wave function $\psi_j(\mathbf{R}_j,t)$, however, one must introduce the notion of time into equation (12) and rewrite it as:

$$\hat{H}(t)=\sum_j\left[-\frac{\hbar^2}{2m}\nabla_j^2+V(\mathbf{R}_j(t))\right]+\frac{1}{2}\sum_{\substack{j,k\\ j\neq k}}\frac{e^2}{4\pi\varepsilon|\mathbf{R}_j(t)-\mathbf{R}_k(t)|} \qquad (13)$$

where $V(\mathbf{R}_j(t))=V_{ext}(\mathbf{R}_j(t))+V_t(\mathbf{R}_j(t),t)$, V_{ext} is the potential due to the positive ions, $V_t\propto e^{i(k_g x-\omega_0 t)}$ is the time-dependent potential due to the creation/anhelation of charge bundles and $\mathbf{R}_j$ is the position vector of the j^{th} electron. Note that by making $\mathbf{R}_{j,k}$ time-dependent, $j\neq k$ is taken care of, however, V_t has both time and spatial dependence (other than that of positive ions). Time-dependent Hamiltonian in Equation (13) implies that the computation must trace the position of each electron, $\mathbf{R}_j$ with respect to t and the changes in potential with respect to t and $\mathbf{R}_j$. The Hartree approximations [23] are also based on time-independent electron-electron interactions, so it must be remedied accordingly for time crystals. An interesting article by Linde [24] may prove to be useful to investigate possible changes to the effective mass and conductivity in an applied field but that also needs to be modified. With the advent of High Performance Computing (HPC) ab initio modelling and simulations of matters where the constituting components are atoms and electrons are becoming more accessible. An article by Borysov *et. al.* [25] provides a background on the existing infrastructure for numerically modelling and investigating structures at atomic levels using the Density Functional Theory (DFT) calculations, which may prove to be a platform of choice to study time crystals.

5. Conclusions

In conclusion, it was shown that for a sufficiently thin silver film sandwiched between two different dielectrics, the mixing of the two SPPs (formed at the substrate and the superstrate) produce an interference envelope that modulates the travelling SPPs. For film thicknesses equivalent to the SPP's penetration depth, surface waves from optically denser dielectric/metal interface would dominate, leading to volume plasmons that propagate inside the film at optical frequencies. Interference of such volume charges with the incident field over the span of the film creates charge bundles that are periodic in space and time. Although many questions remained unanswered in this report, the future work will focus on them. I would hypothesize that the presence of charge bundles inside the film may imply changes to the electronic density of states, electron-electron collision (hence the mean free path), electron-lattice interaction (hence the electron's effective mass) and consequently conductivity, due to the presence of an additional periodic potential that may compete or superpose with that of the positive ions. It is intuitive to think of the periodic "0"s as loci where electrons trapped. If this hypothesis is validated by experiment, it would open doors to study new phenomena. Each "0" may be viewed as super-atom with oversaturated electronic orbitals, elevated fermi level, lowered work function and many more effects when considered in periodic settings which are analogous to that of a superlattice in semiconductors[23].

Funding sources: There were no founding sponsors supporting this work.

Conflicts of Interest: The authors declare no conflict of interest. Apart from the named author, no other person or entity had any role in the inception or the design of the study; in the collection, analysis, or interpretation of data; in the writing of the manuscript, and in the decision to publish the results.

Appendix A – Superposition

To explain the overlap between the beat modulation and the second harmonics in the envelope when $n_1 = 2.41$ at $\lambda_0 = 700$ nm, consider the superposition of two waves having equal amplitudes propagating along the x-axis i.e. $\Psi(x,t) = e^{i(k_1 x - \omega_1 t)} + e^{i(k_2 x - \omega_2 t)}$, which can be written as:

$$\Psi(x,t) = 2e^{i\left(\frac{(k_1+k_2)x}{2} - \frac{(\omega_1+\omega_2)t}{2}\right)} \cos\left(\frac{(k_1-k_2)x}{2}\right)\cos\left(\frac{(\omega_1-\omega_2)t}{2}\right) \qquad \text{(A1)}$$

Here it is assumed both waves start in phase. This form of the equation is of interest since it separates the terms related to the coherent length, $4\pi/(k_1+k_2)$, and the coherent time, $4\pi/(\omega_1+\omega_2)$ of the superposed travelling wave. Furthermore, the last two cosine terms indicate that the combined travelling wave is modulated by two envelopes having nodes (or anti-nodes) separated by $\left|\cos\left(\frac{(k_1-k_2)x}{2}\right)\right|$ in space and $\left|\cos\left(\frac{(\omega_1-\omega_2)t}{2}\right)\right|$ in time. In other words the beat frequencies in space and time are $|k_1-k_2|$ and $|\omega_1-\omega_2|$ respectively, therefore the coherent lengths (for a lack of a better word) of the envelopes in space and time can be calculated as $2\pi/(k_1-k_2)$ and $2\pi/(\omega_1-\omega_2)$ respectively. Necessary conditions to eliminate undesirable jitters in space and time envelopes are:

$$[2\pi/(k_1-k_2)] = [4\pi/(k_1+k_2)] \qquad \text{(A2)}$$

AND

$$[2\pi/(\omega_1-\omega_2)] = [4\pi/(\omega_1+\omega_2)] \qquad \text{(A3)}$$

In the case of two superposed SPP waves at the air/silver interface, the superposition may be simplified to:

$$\sigma(x,t) = e^{-i\omega_0 t}\left[C_a e^{i(k_a x)} + C_{\delta g} e^{i(k_g x)}\right] \qquad \text{(A4)}$$

Furthermore, in the case of 25 nm silver film $C_{\delta g} \approx C_a$, see Figure 2(c) and (e). Under such conditions, equation (A4) may be written for the spatial terms as:

$$\sigma(x) = \left[2e^{i\left(\frac{(k_a+k_g)x}{2}\right)}\cos\left(\frac{(k_a-k_g)x}{2}\right)\right] \qquad \text{(A5)}$$

Equation(A5), which is the special case of equation(A1), shows the coherent length of the combined travelling SPP waves to be $4\pi/(k_a+k_g)$ with the beat modulation occurring according to $2\pi/|k_a-k_g|$. A necessary condition to overlap the coherent length and the beat modulation with the second harmonics in the envelope is then:

$$1/2k_a = 2\pi/|(k_a-k_g)| = 4\pi/(k_a+k_g) \qquad \text{(A6)}$$

Preprints (www.preprints.org) | NOT PEER-REVIEWED | Posted: 29 April 2018 doi:10.20944/preprints201801.0173.v4

In this report, numerical values for wavenumbers obtained from FFT showed $1/2K_a \approx 1/|K_a - K_g| \approx 2/|K_a + K_g|$ at $\lambda_0 = 700$ nm when $n_1 = 2.41$. Clearly in the case of a glass substrate with $n_1 = 1.52$, $1/2K_a \neq 1/|K_a - K_g| \neq 2/|K_a + K_g|$ at $\lambda_0 = 700$ nm.

The appendix is an optional section that can contain details and data supplemental to the main text. For example, explanations of experimental details that would disrupt the flow of the main text, but nonetheless remain crucial to understanding and reproducing the research shown; figures of replicates for experiments of which representative data is shown in the main text can be added here if brief, or as Supplementary data. Mathematical proofs of results not central to the paper can be added as an appendix.

Appendix B - Lorentz Force and Induce Charges Inside the Film

Let the magnetic flux density and the electric field carried by SPPs be denoted by:

$$\mathbf{B}_{\mathrm{m}} = \left(0, B_y, 0\right) e^{i(k_x x + k_z z - \omega_0 t)} \qquad \text{(B1)}$$

$$\mathbf{E}_{\mathrm{m}} = \left(E_x, 0, E_z\right) e^{i(k_x x + k_z z - \omega_0 t)} \qquad \text{(B2)}$$

For simplicity, ignoring the exponent terms, we are interested in $F_x = J_z B_y$ where $J_z = \sigma_e E_z$. Given that $\mathbf{B}_m = \dfrac{\nabla \times \mathbf{E}_m}{j\omega_0}$

and

$$\nabla \times \mathbf{E}_m = \begin{pmatrix} \partial_x \\ \partial_y \\ \partial_z \end{pmatrix} \times \begin{pmatrix} E_x \\ 0 \\ E_z \end{pmatrix} = \begin{pmatrix} \partial_y E_z \\ -\partial_x E_z + \partial_z E_x \\ \partial_y E_x \end{pmatrix} \qquad \text{(B3)}$$

In 2D:

$$\nabla \times \mathbf{E}_m = \begin{pmatrix} 0 \\ -ik_x E_z + ik_z E_x \\ 0 \end{pmatrix} \qquad \text{(B4)}$$

One can write $B_y = \dfrac{k_x E_z - k_z E_x}{\omega_0}$. The Lorentz force distribution along the x-axis is then $F_x = J_z B_y = \sigma_m E_z \dfrac{k_x E_z - k_z E_x}{\omega_0}$. This can be further reduced by $E_x = -i\sqrt{\dfrac{-\varepsilon_m}{\varepsilon_d}} E_z$ to:

$$F_x = \frac{\sigma_m}{\omega_0}\left[k_x + k_z\left(i\sqrt{\frac{-\varepsilon_m}{\varepsilon_d}}\right)\right]E_z^2 \qquad \text{(B5)}$$

Using equations (1)-(2) and replacing $\sigma_m = \omega_0 \varepsilon_0 \varepsilon''_m$ [26], the Lorentz force becomes:

$$F_x = \frac{\omega_0 \varepsilon_0 \varepsilon''_m}{c}\left[\frac{\sqrt{\varepsilon_m \varepsilon_d} + i\varepsilon_m\sqrt{\dfrac{-\varepsilon_m}{\varepsilon_d}}}{\sqrt{\varepsilon_m + \varepsilon_d}}\right]E_z^2 \qquad \text{(B6)}$$

The volume charge profile along the x-direction due to only the Lorentz force may be calculated as $\Delta\rho_x = F_x / E_x$ where $E_x = -i\sqrt{\dfrac{-\varepsilon_m}{\varepsilon_d}} E_z$, therefore:

$$\Delta\rho_x = -\frac{\omega_0}{c}\varepsilon_0\varepsilon_m^{"}\left[\frac{\varepsilon_d+\varepsilon_m}{\sqrt{\varepsilon_m+\varepsilon_d}}\right]E_z \quad \text{(B7)}$$

And in terms of number of free electrons:

$$\Delta N = \frac{\Delta\rho_x}{e^-} = -\frac{\omega_0}{ce^-}\varepsilon_0\varepsilon_m^{"}\left[\frac{\varepsilon_d+\varepsilon_m}{\sqrt{\varepsilon_m+\varepsilon_d}}\right]E_z \quad \text{(B8)}$$

References

1. Wang, L.M.; Zhang, L.X.; Seideman, T.; Petek, H. Dynamics of coupled plasmon polariton wave packets excited at a subwavelength slit in optically thin metal films. *Phys. Rev. B* **2012**, *86*.
2. Verhagen, E.; Dionne, J.A.; Kuipers, L.; Atwater, H.A.; Polman, A. Near-field visualization of strongly confined surface plasmon polaritons in metal-insulator-metal waveguides. *Nano Lett.* **2008**, *8*, 2925-2929.
3. Davis, T.J. Surface plasmon modes in multi-layer thin-films. *Opt. Commun.* **2009**, *282*, 135-140.
4. Berini, P. Long-range surface plasmon polaritons. *Advances in Optics and Photonics* **2009**, *1*, 484-588.
5. Ortuno, R.; Garcia-Meca, C.; Rodriguez-Fortuno, F.J.; Marti, J.; Martinez, A. Role of surface plasmon polaritons on optical transmission through double layer metallic hole arrays. *Phys. Rev. B* **2009**, *79*.
6. Djalalian-Assl, A. Optical nano-antennas. PhD, The University of Melbourne, Melbourne, 2015.
7. Novotny, L.; Hecht, B. *Principles of nano-optics*. Cambridge, U.K. : Cambridge University Press, 2006.: 2006.
8. Rosa, A.L. Lectures 9: Surface plasmon polaritons. http://web.pdx.edu/~larosaa/Applied_Optics_464-564/Lecture_Notes_Posted/2010_Lecture-7_SURFACE%20PLASMON%20POLARITONS%20AT%20%20METALINSULATOR%20INTERFACES/Lecture_on_the_Web_SURFACE-PLASMONS-POLARITONS.pdf
9. Palik, E.D. *Handbook of optical constants of solids*. Academic Press: San Diego, 1985; p 350.
10. Dai, W.; Soukoulis, C.M. Theoretical analysis of the surface wave along a metal-dielectric interface. *Phys. Rev. B* **2009**, *80*, 155407.
11. Nikitin, A.Y.; Garcia-Vidal, F.J.; Martin-Moreno, L. Surface electromagnetic field radiated by a subwavelength hole in a metal film. *Phys. Rev. Lett.* **2010**, *105*.
12. Main, I.G. *Vibrations and waves in physics*. Cambridge University Press: 1987.
13. Phillip, H.R.; Taft, E.A. Kramers-kronig analysis of reflectance data for diamond. *Physical Review a-General Physics* **1964**, *136*, 1445-&.
14. Fairchild, B.A.; Olivero, P.; Rubanov, S.; Greentree, A.D.; WaIdermann, F.; Taylor, R.A.; Walmsley, I.; Smith, J.M.; Huntington, S.; Gibson, B.C., *et al.* Fabrication of ultrathin single-crystal diamond membranes. *Adv. Mater.* **2008**, *20*, 4793-4798.
15. Fu, Y.; Zhou, W.; Lim, L.E.N.; Du, C.L.; Luo, X.G. Plasmonic microzone plate: Superfocusing at visible regime. *Appl. Phys. Lett.* **2007**, *91*.
16. Chen, W.B.; Abeysinghe, D.C.; Nelson, R.L.; Zhan, Q.W. Plasmonic lens made of multiple concentric metallic rings under radially polarized illumination. *Nano Lett.* **2009**, *9*, 4320-4325.
17. Eisberg, R.M.; Resnick, R. *Quantum physics of atoms, molecules, solids, nuclei, and particles*. 2nd ed.; Wiley: New York, 1985.
18. Djalalian-Assl, A. Dipole emission to surface plasmon-coupled enhanced transmission in diamond substrates with nitrogen vacancy center- near the surface. *Photonics* **2017**, *4*, 10.
19. Wilczek, F. Quantum time crystals. *Phys. Rev. Lett.* **2012**, *109*, 5.
20. Shapere, A.; Wilczek, F. Classical time crystals. *Phys. Rev. Lett.* **2012**, *109*, 4.
21. Ashcroft, N.W.; Mermin, N.D. *Solid state physics*. Holt: New York,, 1976; p xxi, 826 p.
22. Blu¨mel, R. *Advanced quantum mechanics the classical-quantum connection*. Jones and Bartlett Publishers: Sudbury, Mass., 2011; p xii, 425 p.
23. Davies, J.H. *The physics of low-dimensional semiconductors : An introduction*. Cambridge University Press: Cambridge, U.K. ; New York, NY, USA, 1998; p xviii, 438 p.
24. Linde, J.O. The effective mass of the conduction electrons in metals and the theory of superconductivity. *Physics Letters* **1964**, *11*, 199-201.
25. Borysov, S.S.; Geilhufe, R.M.; Balatsky, A.V. Organic materials database: An open-access online database for data mining. *Plos One* **2017**, *12*, 14.

 doi:10.20944/preprints201801.0173.v4

26. Lorrain, P.; Corson, D.R.; Lorrain, F. *Electromagnetic fields and waves : Including electric circuits*. Freeman: New York, 1988.